Graphical Abstract

To create your abstract, type over the instructions in the template box below.
Fonts or abstract dimensions should not be changed or altered.

Optical properties of highly planar Diketopyrrolopyrrole derivatives fixed by coordinate bonds

Leave this area blank for abstract info.

Takuya Yamagata, Junpei Kuwabara, Takaki Kanbara*
Tsukuba Research Center for Interdisciplinary Materials Science (TIMS), Graduate School of Pure and Applied Sciences University of Tsukuba, 1-1-1 Tennodai, Tsukuba 305-8573, Japan

Tetrahedron
journal homepage: www.elsevier.com

Optical properties of highly planar Diketopyrrolopyrrole derivatives fixed by coordinate bonds

Takuya Yamagata, Junpei Kuwabara, and Takaki Kanbara*

Tsukuba Research Center for Interdisciplinary Materials Science (TIMS), Graduate School of Pure and Applied Sciences, University of Tsukuba, 1-1-1 Tennodai, Tsukuba 305-8573, Japan

ARTICLE INFO

Article history:
Received
Received in revised form
Accepted
Available online

Keywords:
Diketopyrrolopyrrole
boron complex
platinum complex
UV/Vis spectroscopy

ABSTRACT

Diketopyrrolopyrrole (DPP) derivatives bearing 2-pyridyl groups were synthesized, which could serve as anionic *N,N'*-chelate ligands consisting of two nitrogen atoms of the lactam moieties and the pyridyl groups. Coordination of the DPP ligand to boron and platinum yielded the corresponding DPP complexes. Their crystal structures exhibited coplanar structures between the DPP core and the 2-pyridyl groups, which indicated extended π-conjugation. The maximum absorption wavelength of the DPP complexes was longer than that of the corresponding DPP ligands. The choice of the introduced element affects the optical properties of the DPP complexes; the platinum complex has a longer absorption wavelength than the boron complex. The theoretical calculation revealed that these absorptions can be attributed to the π-π* transition. The introduction of the coordinating elements predominantly lowers the band gap. In addition, the substituent on the 2-pyridyl group can also modulate the energy levels.

1. Introduction

Diketopyrropyrrole (DPP) is a pigment consisting of a condensed lactam core flanked by aromatic rings such as phenyl and thienyl groups. Owing to the high molar absorbance coefficient and high fluorescence quantum yields of the DPP derivatives, applications in bioimaging have been developed in recent years.[1] Moreover, DPP derivatives bearing molecular recognition parts have been used as chemosensors.[2,3] Polymers and oligomers containing DPP units have also been recognized as promising materials in organic thin-film transistors[4] and organic solar cells.[5] To obtain high performance materials in synthetic research, one of the most important targets to achieve is the facile modulation of energy levels.[6,7] Energy levels are generally controlled by the introduction of substituents such as electron donating or electron withdrawing groups on the starting compounds' aromatic groups. However, in some cases, the effects of the substituent were limited. For example, change from an electron withdrawing substituent to an electron donating one resulted in only a 50 nm-shift in the absorption maximum of a DPP derivative.[6] The limited substituent effects are likely caused by the twisted structures between the condensed lactam moieties (DPP core) and the flanked phenyl groups.[8] Because this distortion prevents the extension of π-conjugation between the DPP core and the aromatic groups, inhibition of the distortion is considered to afford significant effects on the energy levels owing to the effectively extended π-conjugation. Indeed, Gryko et. al. reported a carbon-bridged coplanar structure in the DPP derivative affording a large bathochromic shift in absorption.[9] Regarding the construction of a rigid coplanar skeleton, a coordinate bond can be used instead of a covalent bond.[10] The coordinate bonds between B and N have been known to provide π-conjugated ladder molecules with boron-bridging structures.[11] The introduced boron element also affects electronic properties; e.g., it increases the electron affinity.[11a,b,c] If the coordinating elements can be introduced at the last synthetic step, several types of DPP derivatives, having different energy levels, can be prepared from one building block. Therefore, we focused on fixing a π-conjugated framework in a planar fashion using coordinate bonds (Fig. 1). Herein, we report the syntheses of DPP derivatives bearing a coplanar skeleton, using coordinate bonds. The effects of coordinating elements and substituents were investigated in terms of absorbing properties and energy levels.

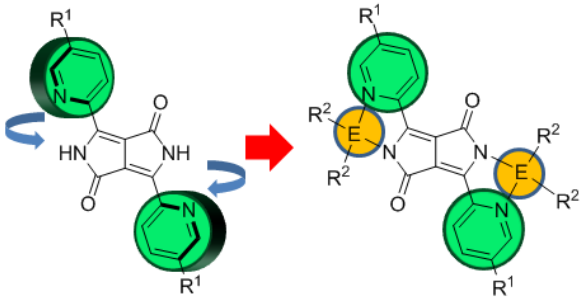

Fig. 1. DPP complex.

2. Results and discussion

2.1. Synthesis

DPP derivatives bearing 2-pyridyl groups (H-DPP) were selected as an *N,N′*-chelate ligand consisting of the nitrogen atoms of the lactam and pyridyl groups. H-DPP[12] was synthesized in 60% yield by a cyclization reaction of 2-cyanopyridine with di-*n*-butylsuccinate in the presence of sodium in *tert*-amylalcohol (Scheme 1). Similarly, Br-DPP and Pip-DPP were synthesized in 18% and 56% yields from 5-bromo-2-cyanopyridine and 2-cyano-5-(1-piperidinyl)pyridine, respectively. The reactions of H-DPP, Br-DPP, and Pip-DPP with BPh_3 in toluene at reflux temperature afforded H-B-DPP, Br-B-DPP, and Pip-B-DPP in 71%, 21%, and 60% yields, respectively. Br-DPP is a lower yield than H-DPP and Pip-DPP due to the low solubility and side-reactions. The platination reaction of H-DPP with *cis*-$PtCl_2(dmso)_2$ and the subsequent reaction with dipivaloylmethane afforded H-Pt-DPP in 4% yield (Scheme 2). Dipivaloylmethane, bearing the bulky ^{t}Bu groups, was introduced as assistance ligands in order to increase solubility because compounds bearing rigid coplanar skeletons generally have low solubility.[9]

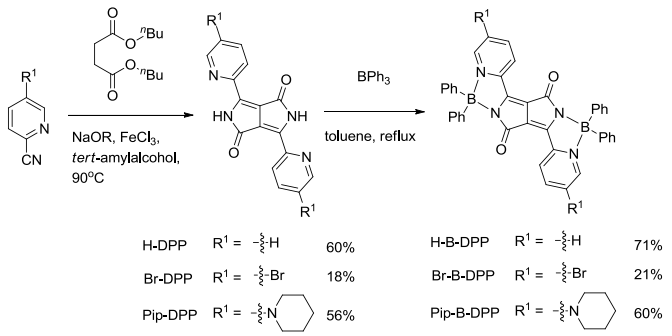

Scheme 1. Syntheses of DPP boron complexes.

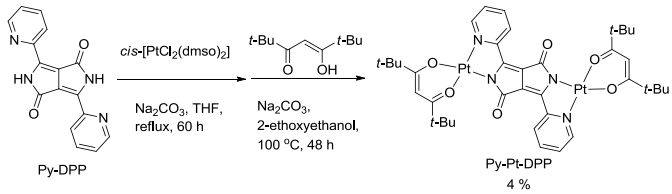

Scheme 2. Synthesis of H-Pt-DPP.

2.2. Solid –state structure

The solid-state molecular structures of H-B-DPP and H-Pt-DPP were determined by X-ray diffraction analysis. The crystal structures of H-B-DPP and H-Pt-DPP are shown in Fig. 2. The dihedral angle of H-B-DPP between the DPP core and the 2-pyridyl groups is 1.75°, and that of H-Pt-DPP is 2.74°. These results show that the DPP complexes have a coplanar skeleton. The average dihedral angle of H-DPP is 6.01°, which is estimated from the reported crystal structure.[13] These comparisons revealed that the planarity of the DPP complexes is higher than that of H-DPP. Intermolecular interactions such as π-π stacking were not observed in the packing diagrams because the H-B-DPP and H-Pt-DPP contain bulky phenyl groups or ^{t}Bu groups (Fig. S13 and S14 in Supplementary data).

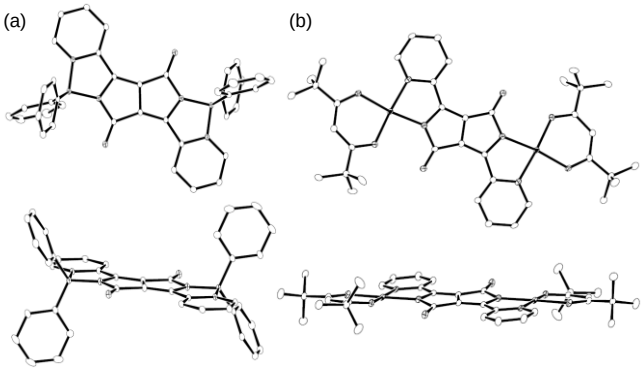

Fig. 2. ORTEP drawings of (a) H-B-DPP, (b) H-Pt-DPP with thermal ellipsoids shown at the 30% probability level. Hydrogen atoms and solvated chloroform and hexane molecules are omitted for clarity.

2.3. UV/Vis absorption spectroscopy

The UV/Vis absorption spectra of the obtained compounds were measured in $CHCl_3$ (Figs. 3 and 4). The photophysical properties of the compounds are summarized in Table 1. The spectra of DPP derivatives show two vibronic maxima, the 0-0 vibronic transition being more intensive than 0-1.[14] The maximum absorption wavelength (λ_{max}) of H-B-DPP bearing boron centers was 113 nm longer than that of H-DPP (Fig. 3). In the case of the platinum complex, H-Pt-DPP, a bathochromic shift of 181 nm was observed when compared with H-DPP. These bathochromic shifts resulting from the formation of coordinate bonds were considerably larger (113, 181 nm) than those from the introduction of substituents on the phenyl groups (50 nm).[6] A platinum complex with a monodentate DPP ligand at the lactam nitrogen has been reported (Fig. S15a).[8] Because the λ_{max} of the DPP complex showed absorption at 536 nm, the absorption in the long wavelength region of H-Pt-DPP occurred because of the bidentate coordination, resulting in a coplanar structure and extension of π-conjugation. Moreover, because the bathochromic shift of H-Pt-DPP was larger than that of H-B-DPP, the absorption properties of the complex could be modulated by choosing suitable coordinating elements.

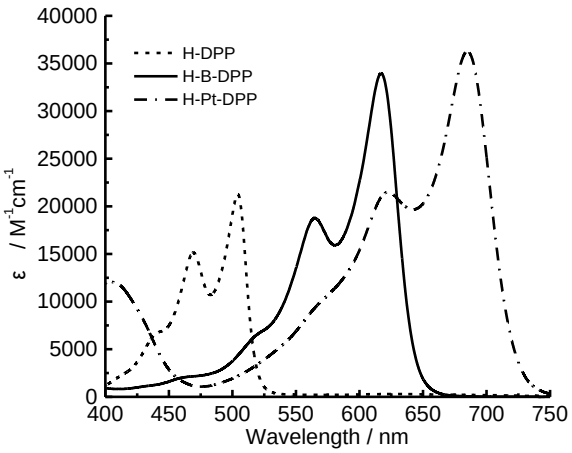

Fig. 3. UV/ Vis absorption spectra of DPP derivatives (in $CHCl_3$).

We measured the UV/Vis abortion spectra in DMSO (Fig. S20). In the case of H-DPP, λ_{max} in DMSO was 11 nm longer than that in $CHCl_3$. In contrast, λ_{max} of H-B-DPP and H-Pt-DPP in DMSO were ca. 15 nm shorter than that in $CHCl_3$. These results indicate that a polarization of the ground state of H-B-DPP and H-Pt-DPP is larger than that of H-DPP.

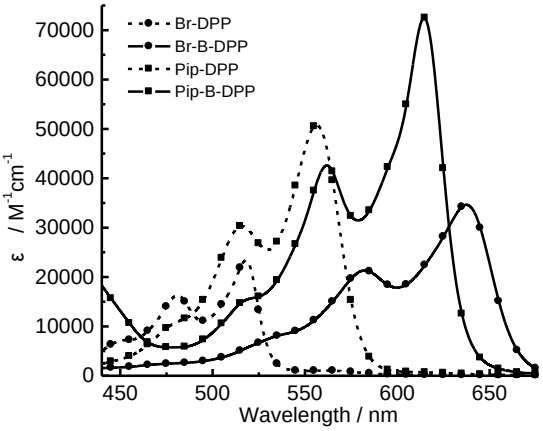

Fig. 4. UV/Vis absorption spectra of DPP derivatives (in $CHCl_3$).

Bathochromic shifts by coordination of boron were also observed in the Br-B-DPP and Pip-B-DPP bearing substituents on the 2-pyridyl groups (Fig. 4 and Table 1). The λ_{max} of Br-B-DPP was 120 nm longer than that of Br-DPP. In contrast, the λ_{max} of Pip-B-DPP exhibited a 59-nm bathochromic shift from Pip-DPP. These results showed that the degree of bathochromic shift by coordination of boron depends on the substituents. The molar absorbance coefficient (ε) of the DPP complexes was approximately 1.5 times larger than that of the corresponding DPP ligands, indicating that the extension of the length of the π-conjugation system also contributed to the increase in the molar absorption coefficient.

2.4. Time-dependent density theory calculations

To elucidate the relationship between the absorption properties and the coordinating elements or the substituents on the 2-pyridyl groups, DPP derivatives were examined by performing theoretical calculations. After optimization of the geometric structures, time-dependent density theory (TD-DFT) calculations were performed in the Gaussian 09 program suite.[15] Fig. 5 shows molecular orbitals of the DPP derivatives. The lowest unoccupied molecular orbital (LUMO) of H-DPP was extended on the DPP core and the 2-pyridyl groups. In contrast, the highest occupied molecular orbital (HOMO) was almost localized on the DPP core and the contribution of the 2-pyridyl groups was small. Similar trends were observed in the HOMO and LUMO of H-B-DPP and H-Pt-DPP. The results of the TD-DFT calculations indicated that absorption in the long wavelength region was attributed to transitions from the HOMO to the LUMO, which were assigned as π-π* transitions (see Figs. S21 and S22, and Table S1).

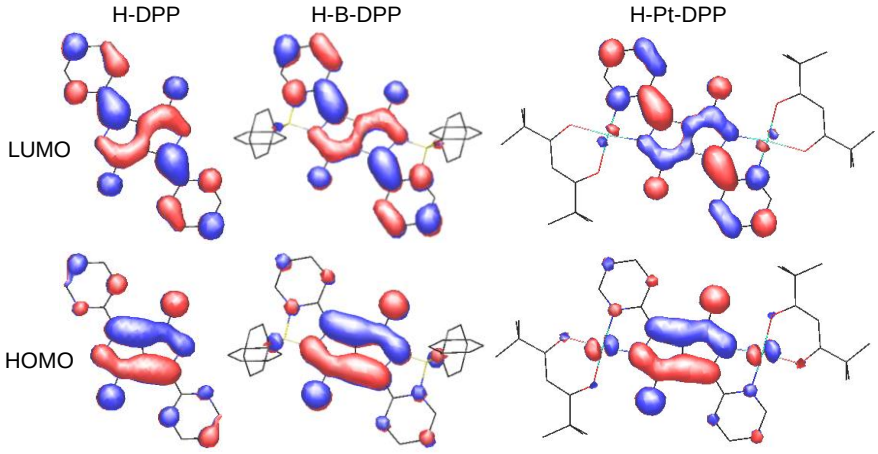

Fig. 5. Molecular orbitals of DPP derivatives.

Table 1
Photophysical properties of DPP derivatives

	UV[a]		Simulated	Emission[c]	Stokes shift
	λ_{max} / nm	ε / $Lmol^{-1}cm^{-1}$	λ_{max}[b] / nm	λ_{em} / nm	in solution / cm^{-1}
H-DPP	504	21100	483	514	386
H-B-DPP	617	34000	639	638	533
H-Pt-DPP	685	36300	699	-	-
Br-DPP	518	23500	498	527	330
Br-B-DPP	638	34600	661	662	568
Pip-DPP	556	50800	506	576	625
Pip-B-DPP	615	72500	614	632	437

[a] UV/Vis absorption spectra were measured in chroloform.
[b] The wavelength of maximum absorption simulated by DFT calculation.
[c] Emission spectra were measured with excitation at λ_{max} in UV/Vis absorption in chroloform.

The HOMO and LUMO levels are summarized in Table 2. The values of the calculated band gaps (E_g^{calcd}) are in good agreement with those of the experimentally obtained optical band gaps (E_g^{opt}). The HOMO levels of H-B-DPP and H-Pt-DPP are higher than those of H-DPP, and the LUMO levels of the DPP complexes are lower than those of H-DPP. These results show that both the HOMO and LUMO levels contributed to the narrowed band gaps of the DPP complexes. As shown in Fig. 3, the λ_{max} of H-Pt-DPP appears at a longer wavelength than that of H-B-DPP. To consider the origin of the wide band gap of H-B-DPP, the energy levels are compared between H-B-DPP and H-Pt-DPP. Both the HOMO and LUMO levels of H-B-DPP are lower than those of H-Pt-DPP (Table 2, Fig. S17). The decrease in the HOMO level in H-B-DPP is more significant (-0.37 eV) than that of the LUMO level (-0.22 eV). The significant decrease in the HOMO level provides the wide band gap of H-B-DPP in comparison with H-Pt-DPP. High Lewis acidity of the boron center is likely to contribute to lowering the HOMO level. The literature reports imine-introduced indigo derivatives, named as Nindigo, which have served as β-diketiminate-type ligands consisting of nitrogen atoms on the indigo moiety and the imine groups.[16] The Nindigo complexes with boron centers (Fig. S15b) possess a lower HOMO level (-5.60 eV) than those with palladium centers (-4.88 eV), with the HOMO and LUMO values being estimated from oxidation potentials in cyclic voltammetry.[16c] The low HOMO level of Nindigo complexes with the boron center suggests that the relatively low HOMO level of H-B-DPP is a general trend. These results indicate that relatively weak Lewis acidity of platinum provide bathochromic shifts in comparison with boron.

Table 2
HOMO-LUMO energies and energy band gaps of DPP derivatives on the basis of the TD-DFT calculation

	HOMO	LUMO	E_g^{calcd} [c]	E_g^{opt} [d]
H-DPP[a]	-5.41 eV	-2.76 eV	2.57 eV	2.40 eV
H-B-DPP[a]	-5.24 eV	-3.17 eV	1.94 eV	1.93 eV
H-Pt-DPP[b]	-4.87 eV	-2.95 eV	1.77 eV	1.72 eV
Br-DPP[a]	-5.63 eV	-3.05 eV	2.49 eV	2.32 eV
Br-B-DPP[a]	-5.37 eV	-3.36 eV	1.88 eV	1.86 eV
Pip-DPP[a]	-4.72 eV	-2.19 eV	2.45 eV	2.14 eV
Pip-B-DPP[a]	-4.71 eV	-2.56 eV	2.02 eV	1.94 eV

[a] Time-dependent density functional theory (TD-DFT) calculations were performed at the B3LYP level with the 6-31G(dp)
[b] TD-DFT calculation was performed at the B3PW91 level with the LanL2DZ.
[c] Calculated by TD-DFT.
[d] Estimated by UV-Vis absorption spectroscopy.

The effects of substituents on the band gaps and energy levels were also examined on the basis of the results of the theoretical calculations. Although both the HOMO and LUMO of Br-DPP were at lower energy levels than those of H-DPP (Fig. S19a), the difference in the LUMOs between H-DPP and Br-DPP was more significant (0.29 eV) than that between their HOMOs (0.22 eV). In contrast, electron-donating piperidyl groups strongly affect the HOMO, resulting in the narrow energy band gap. Therefore, the λ_{max} of Br-DPP and Pip-DPP are longer than that of H-DPP. In the case of boron complexes, the substituent effects on the band gaps are considered to be small, because the band gap of H-B-DPP (1.94 eV) is similar to those of Br-B-DPP (1.88 eV) and Pip-B-DPP (2.02 eV). This small dependence of the band gaps on the substituents is quite a contrast to the above-mentioned strong effects of the introduction of B or Pt. However, the substituents strongly affected the energy levels; the order of HOMO and LUMO levels was the same as the order of electron donating ability of the substituent (Pip-B-DPP > H-B-DPP > Br-B-DPP, Fig. S19b), which correlates with the pristine DPP derivatives. These results indicate that electron donating ability of the substituents provide the increase in the energy levels; the choice of the substituent on the 2-pyridyl group can also modulate HOMO and LUMO levels.

2.5. Electrochemical properties

Cyclic voltammetry measurements were performed in order to evaluate the electrochemical properties and confirm the energy levels of the DPP derivatives by experimental investigations. The redox potentials are summarized in Table 3. All DPP derivatives exhibited reversible reduction waves in the negative potential region (see Fig. S23). The first half-wave reduction potentials ($E_{1/2}^{1red}$) of H-B-DPP and H-Pt-DPP [-1.089 and -1.168 V vs. Fc^+/Fc (ferrocenium/ferrocene)] were less negative than that of H-DPP [-1.396 V vs. Fc^+/Fc]. These results suggested that the boron p orbital and the platinum d orbital withdraws electron from the DPP core. Because the Lewis acidity of boron is higher than that of platinum, the $E_{1/2}^{1red}$ of H-B-DPP was less negative than that of H-Pt-DPP. Moreover, DPP complexes showed second reversible reduction waves because of their increased electron affinity (Table 3).[17]

Table 3
Electrochemical data[a] for DPP derivatives

	$E_{1/2}^{1red}$ [V][b]	$E_{1/2}^{2red}$ [V][b]	HOMO[c]	LUMO[d]
H-DPP	-1.396		-5.87	-3.47
H-B-DPP	-1.089	-1.585	-5.72	-3.79
H-Pt-DPP	-1.168	-1.647	-5.29	-3.57
Br-DPP	-1.281		-5.91	-3.59
Br-B-DPP	-0.962	-1.384	-5.70	-3.84
Pip-DPP	-1.656		-5.37	-3.23
Pip-B-DPP	-1.348	-1.791	-5.48	-3.54

[a] Redox potentials were measured in DMF ($1x10^{-3}$ M) containing Bu_4NPF_6 (0.1 M). Sweep rate = 100 mVs^{-1}. Potential in V *vs.* Fc^+ / Fc.
[b] Half wave potential.
[c] Determined from the LUMO levels and E_g^{opt} using the equation (HOMO = LUMO - E_g^{opt}).
[d] Determined from the onset potentials of the reduction wave (*vs.* Fc^+ / Fc) using the equation (LUMO = -4.80 - E_{onset}^{red}).

The substituent on the 2-pyridyl group directly affected the reduction potential; Br-B-DPP, which contained the electron withdrawing substituents, had the least negative reduction potential (-0.962 V), and Pip-B-DPP, which contained the electron-donating substituent, had a more negative reduction potential (-1.348 V) than that of H-B-DPP. The LUMO levels were estimated according to the equations LUMO = -(4.80 + E_{onset}^{red}) eV (Table 3).[5b] The HOMO levels of the DPP derivatives were empirically calculated from their LUMO levels and optical band gap (E_g^{opt}).[11c] Although there are differences between the

HOMO and LUMO data estimated from the electrochemical measurements (Table 3) and those from the DFT calculations (Table 2), the trends of the HOMO and LUMO levels were consistent.

2.6. Emission spectra

Fig. 6 shows the emission spectra of the DPP derivatives in chloroform. The maximum emission (λ_{em}) of boron complexes was observed at a wavelength of 632–662 nm. These emission bands presumably originate from a π-π* emission on the DPP chromophore. The maximum emission of H-B-DPP was 124 nm longer than that of H-DPP. The order of λ_{em} was the same as that of the order of absorption (H-B-DPP < Pip-B-DPP < Br-B-DPP). Br-B-DPP exhibited an emission at 662 nm, with the shoulder peak at 723 nm, which is close to the near infrared region. In contrast, H-Pt-DPP did not emit at room temperature. This behavior is the same as that shown by the reported Pt complex with the monodentate DPP ligand (Fig. S15a).[8b]

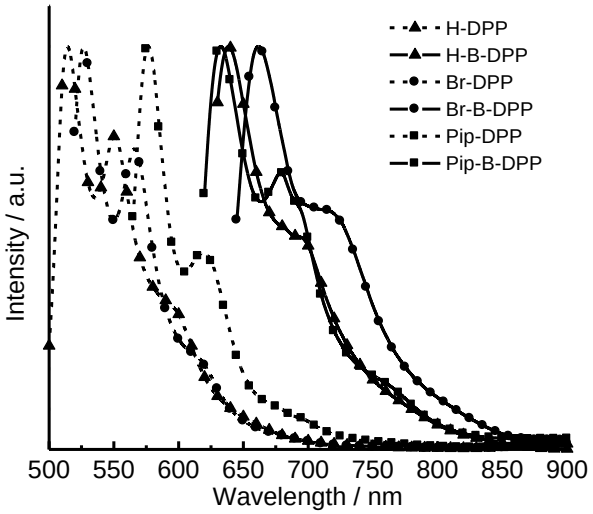

Fig. 6. Normalized emission spectra in $CHCl_3$.

3. Conclusion

Herein, we synthesized DPP complexes with coordinate bonds to boron and platinum. The coordinate bonds provided coplanar structures and extended the π-conjugation, resulting in the bathochromic shifts of absorption and a high molar absorbance coefficient. Because the bathochromic shift of the platinum complex was more significant than that of the boron complex, we concluded that the introduction of the coordinating elements predominantly lowers the band gap of the DPP complex. Moreover, the choice of the substituent on the 2-pyridyl group can also modulate the energy levels. We revealed a strategy for controlling the band gaps and energy levels of the DPP molecules by choosing suitable coordinating elements and substituents. This strategy for fine-tuning the energy levels enables the rational design of novel dye-based materials with suitable optical properties and energy levels.

4. Experimental

4.1. Materials

Tris(dibenzylideneacetone)dipalladium (0) [$Pd_2(dba)_3$] was purchased from Strem Chemicals, Inc. 2-Dicyclohexylphosphino-2',4',6'-triisopropylbiphenyl (XPhos) was purchased from Sigma-Aldrich. *cis*-Dichloro-bis(dimethylsulfoxide)platinum (II) [*cis*-$PtCl_2(dmso)_2$] was prepared according to the literature method.[18] Other chemicals were purchased and used without further purification.

4.2. General Experimental Procedures

NMR spectra were recorded on Bruker AVANCE-400, 600, and JNM-ECS-400 NMR spectrometers. IR spectra were recorded on a JASCO FT/IR-300. Elemental analysis was carried out with a Perkin-Elmer 2400 CHN Elemental Analyzer. UV-vis spectra were recorded on a JASCO V-630iRM spectrophotometer. Emission spectra were recorded on a FP-6200 spectrophotometer. MALDI-MS spectra were recorded on Applied Biosystems SCIEX TOF/TOF™ 5800. HRMS (ESI) spectra were recorded on UPLC/Synapt G2 HDMS. Melting points were measured on a Yanaco MP-500D.

4.3. Crystal structure determination

Intensity data were collected on a Bruker SMART APEX II ULTRA with Mo-*K*α radiation. A full matrix least-squares refinement was used for non-hydrogen atoms with anisotropic thermal parameters method by SIR-92 (H-B-DPP) and SIR-97 (H-Pt-DPP) program. Hydrogen atoms were placed at the calculated positions and were included in the structure calculation without further refinement of the parameters. CCDC-966652 (for H-B-DPP) and CCDC-966651 (for H-Pt-DPP) contain the supplementary crystallographic data for this paper. These data can be obtained free of charge from The Cambridge Crystallographic Data Centre via www.ccdc.cam.ac.uk/data_request/cif.

A single crystal of H-B-DPP suitable for X-ray diffraction studies was obtained by slow diffusion of ethanol into a solution of the compound in $CHCl_3$. A single crystal of H-Pt-DPP suitable for X-ray diffraction studies was obtained by slow diffusion of hexane into a solution of the compound in $CHCl_3$.

4.5. Electrochemical measurement

Electrochemical measurements were carried out with a standard three-electrode configuration. tetrabutylammonium hexafluorophosphate (Bu_4NPF_6) (0.1 M) in dimethylformamide (DMF) was used as a supporting electrolyte with platinum wire auxiliary electrodes and carbon working electrodes. All measurements were carried out under a nitrogen atmosphere, and potentials were related to an Ag^+/Ag reference electrode. The potentials were calibrated with ferrocenium/ferrocene redox couple (Fc^+/Fc).

4.6. Computational details.

The geometrical structures were optimized at the B3LYP level for H-DPP, Br-DPP, Pip-DPP, H-B-DPP, Br-B-DPP and Pip-B-DPP with 6-31G (dp) basis set implemented in Gaussian 09 programs suits. The geometrical structures were optimized at the B3PW91 level for Pt-DPP with LanL2DZ basis set implemented in Gaussian 09 programs suits. Using the optimized geometries, TD-DFT calculations were performed to predict their absorptions.

4.7. Synthesis

4.7.1. H-DPP[12]. Under nitrogen atmosphere, sodium (2.76 g, 120 mmol) and $FeCl_3$ (0.126 g 0.78 mmol) in dry *tert*-amyl alcohol (60 mL) were heated at 90 °C until the sodium was dissolved.

The solution was cooled to about 50 °C, then 2-cyanopyridine (6.25 g, 60 mmol) was added, and the mixture was heated to 90 °C. A solution of di-*n*-buthylsuccinate (5.53 g, 24 mmol) in dry *tert*-amyl alcohol (25 mL) was added dropwise for 1 h at 90 °C. After standing for 24 h, acetic acid (25 mL) was added. The mixture was then heated to 120 °C. After standing for 1 h, the precipitate was filtered and washed with water, methanol, and CH_2Cl_2 repeatedly and dried under vacuum to obtain a red solid. Yield: 4.17 g, 60%. ^{1}H NMR (400 MHz, DMSO-d_6, 333 K) δ = 7.54-7.57 (m, 2H), 8.05-8.10 (m, 2H), 8.76 (d, 2H, *J* = 4.4 Hz), 8.97 (d, 2H, *J* = 7.6 Hz); IR (KBr, cm^{-1}) ν_{max} 3222 (NH), 1691 (amide C=O stretch), 1615, 1569, 1480, 1448, 1417; MALDI-MS calcd for $C_{16}H_{11}N_4O_2$ $[M+H]^+$ 291.1; Found 291.1. Anal. calcd for $C_{16}H_{10}N_4O_2$: C 66.20, H 3.47, N 19.30; Found: C 66.10, H 3.55, N 19.33; mp > 300°C.[12]

4.7.2. H-B-DPP. A mixture of H-DPP (29.0 mg, 0.10 mmol) and triphenylborane (122 mg, 0.50 mmol) in toluene (6.0 mL) was stirred for 48 h at reflux temperature under nitrogen atmosphere. After cooling to room temperature, the volatiles were evaporated to dryness in vacuo. The purple solid was purified by column chromatography (silica gel, $CHCl_3$/ethyl acetate 10/1). The product was washed with hexane and dried under vacuum to obtain a purple solid. Yield: 44.1 mg, 71%. ^{1}H NMR (400 MHz, DMSO-d_6) δ = 7.02-7.07 (m, 12H), 7.13-7.16 (m, 8H), 7.77 (t, 2H, *J* = 6.2 Hz), 8.20 (d, 2H, *J* = 7.6 Hz), 8.39 (t, 2H, *J* = 8.2 Hz), 8.69 (d, 2H, *J* = 5.6 Hz); ^{13}C{^{1}H} NMR (100 MHz, DMSO-d_6, 353 K) δ = 114.9, 123.2, 126.2, 126.9, 127.2, 132.2, 134.0, 141.8, 143.4, 144.1, 144.7, 160.0; IR (KBr, cm^{-1}) ν_{max} 3068, 3045 (aromatic C-H stretch), 1658 (amide C=O stretch), 1616, 1562, 1470, 1430; MALDI-MS calcd for $C_{40}H_{29}B_2N_4O_2$ $[M+H]^+$ 619.3; Found 619.3. HRMS (ESI): calcd. For $C_{40}H_{29}B_2N_4O_2$ $[M + H]^+$ 619.2477; found 619.2466.

4.7.3. H-Pt-DPP. A mixture of H-DPP (407 mg, 1.4 mmol), Na_2CO_3 (1.19 g, 11 mmol) and *cis*-Pt(dmso)$_2$Cl$_2$ (1.18 g, 2.8 mmol) in THF (88 mL) was stirred for 64 h at reflux temperature under nitrogen atmosphere. After cooling to room temperature, the volatiles were evaporated to dryness in vacuo. 2-Ethoxyethanol (40mL) and dipivaloyl methane (1.43 μL, 7.0 mmol) was added. The mixture was heated at 120 °C under nitrogen atmosphere and stirred for 48 h. After cooling to room temperature, the mixture was diluted with $CHCl_3$ and water. The organic layer was separated and washed with water and brine. The product was isolated by column chromatography on silica gel using using $CHCl_3$/ethyl acetate (2/1) as an eluent (53.2 mg, 4%). ^{1}H NMR (400 MHz, $CDCl_3$) δ = 1.26 (s, 18H), 1.33 (s, 18H), 5.90 (s, 2H), 7.26-7.32 (m, 2H), 7.98-8.02 (m, 2H), 8.70 (d, 2H, *J* = 5.6 Hz), 8.43 (d, 2H, *J* = 7.6 Hz); ^{13}C{^{1}H} NMR (100 MHz, $CDCl_3$) δ = 28.4, 40.4, 41.7, 93.6, 119.3, 123.7, 125.3, 138.8, 144.7, 153.6, 155.2, 166.2; IR (KBr, cm^{-1}) ν_{max} 2961 (alkane CH stretch), 1637 (amide C=O stretch), 1600, 1554, 1542, 1530, 1496, 1473, 1455, 1395; MALDI-MS calcd for $C_{38}H_{47}N_4O_6Pt_2$ $[M+H]^+$ 1045.3; Found 1045.4. Anal. calcd for $C_{38}H_{46}N_4O_6$ Pt_2: C 43.68, H 4.44, N 5.36; Found: C 43.87, H 4.28, N 5.36; mp 280°C (decomp.).

4.7.4. Br-DPP[5a]. Under nitrogen atmosphere, sodium (385 mg, 17 mmol), $FeCl_3$ (17.3 mg, 0.11 mmol) and dry *tert*-amyl alcohol (8.4 mL) were heated to 90 °C until the sodium was dissolved. 5-bromo-2-cyanopyridine (1.53 g, 8.4 mmol) was added and then the mixture was heated to 90 °C. A solution of di-*n*-buthylsuccinate (769 mg, 3.3 mmol) in dry *tert*-amyl alcohol (3.3 mL) was added dropwise for 1 h. After standing for 24 h, acetic acid (3.3 mL) was added. The mixture was then heated to 120 °C. After standing for 1 h, the precipitate was filtered and washed with water, methanol, hexane and CH_2Cl_2 and dried under vacuum to obtain a dark red solid. Yield: 264 mg, 18%. ^{1}H NMR (400 MHz, DMSO-d_6) δ = 8.40 (d, 2H, *J* = 8.4 Hz), 8.88 (s, 2H), 8.92 (d, 2H, *J* = 8.8 Hz), 11.38 (s, 2H); IR (KBr, cm^{-1}) ν_{max} 3166 (NH), 1645 (amide C=O stretch), 1613, 1458, 1413; MALDI-MS calcd for $C_{16}H_9Br_2N_4O_2$ $[M+H]^+$ 448.9; Found 448.9. Anal. calcd for $C_{16}H_8Br_2N_4O_2$: C 42.89, H 1.80, N 12.50; Found: C 42.51, H 1.41, N 12.31.

4.7.5. Br-B-DPP. A mixture of Br-DPP (44.8 mg, 0.10 mmol) and triphenylborane (121 mg, 0.50 mmol) in toluene (4.0 mL) was stirred for 24 h at reflux under nitrogen atmosphere. After cooling to room temperature, the volatiles were evaporated to dryness in vacuo. The mixture was purified by column chromatography (silica gel, $CHCl_3$/ethyl acetate 5/1). The product was washed with ethanol and hexane repeatedly and dried under vacuum to obtain a blue solid. Yield: 16.6 mg, 21%. ^{1}H NMR (600 MHz, $CDCl_3$) δ = 7.28-7.33 (m, 14H), 7.37 (d, 8H, *J* = 6.6 Hz), 8.27 (d, 2H, *J* = 8.4 Hz), 8.38 (d, 2H, *J* = 8.4 Hz), 8.55 (s, 2H); IR (KBr, cm^{-1}) ν_{max} 3048 (aromatic C-H stretch), 1664 (amide C=O stretch), 1604, 1465, 1432, 1400; MALDI-MS calcd for $C_{40}H_{27}B_2Br_2N_4O_2$ $[M+H]^+$ 777.1; Found 777.1. HRMS (ESI): calcd. For $C_{40}H_{27}B_2Br_2N_4O_2$ $[M + H]^+$ 777.0666; found 777.0674; mp: 293°C (decomp.).

4.7.6. 2-cyano-5-(1-piperidinyl)pyridine. A solution of $Pd_2(dba)_3$ (91.5 mg, 0.10 mmol), XPhos (191 mg, 0.40 mmol), K_3PO_4 (2.12 g, 10 mmol) and 5-bromo-2-cyanopyridine (732 mg, 4.0 mmol) in 1,2-dimethoxyethane (29 mL) was stirred and degassed with nitrogen for 10 min at room temperature. Piperidine (375 mg, 4.4 mmol) was added. The mixture was heated at 80 °C under nitrogen atmosphere and stirred for 24 h. After cooling to room temperature, the product was isolated by column chromatography on silica gel using CH_2Cl_2/Methanol (9/1) as an eluent (yellow oil, 674 mg, 90%). ^{1}H NMR (400 Hz, $CDCl_3$) δ = 1.69 (s, 6H), 3.38 (s, 4H), 7.05 (dd, 1H, *J* = 8.4, 3.2 Hz), 7.47 (d, 1H, *J* = 8.4 Hz), 8.28 (d, 1H, *J* = 2.4 Hz) ; ^{13}C{^{1}H} NMR (100 MHz, $CDCl_3$) δ = 24.0, 25.0, 47.8, 118.5, 118.9, 120. 1, 129.0, 138.0, 148.1; MALDI-MS calcd for $C_{11}H_{14}N_3$ $[M+H]^+$ 188.1; Found 188.1. Anal. calcd for $C_{11}H_{13}N_3$: C 70.56, H 7.00, N 22.44; Found: C 70.32, H 7.26, N 22.09.

4.7.7. Pip-DPP. Under nitrogen atmosphere, sodium (115 mg, 5.0 mmol), $FeCl_3$ (5.2 mg, 0.032 mmol) and dry *tert*-amyl alcohol (2.5 mL) were heated to 90 °C until the sodium was dissolved. 2-cyano-5-(1-piperidinyl)pyridine (468 mg, 2.5 mmol) was added and then the mixture was heated to 90 °C. A solution of di-*n*-buthylsuccinate (230 mg, 1.0 mmol) in dry *tert*-amyl alcohol (2.0 mL) was added dropwise for 2 h. After standing for 24 h, acetic acid (1.0 mL) was added. The mixture was then heated to 120 °C. After standing for 1 h, the precipitate was filtered and washed with water, Methanol and Et_2O repeatedly and dried under vacuum to obtain a purple solid. Yield: 255 mg, 56%. ^{1}H NMR (400 MHz, DMSO-d_6) δ = 1.63 (s, 12H), 3.47 (s, 8H), 7.49 (dd, 2H, *J* = 9.2, 2.8 Hz), 8.38 (d, 2H, *J* = 2.8 Hz), 8.83 (d, 2H, *J* = 9.2 Hz), 10.69 (s, 2H); ^{13}C{^{1}H} NMR (100 MHz, DMSO-d_6) δ = 23.8, 24.8, 47.4, 108.9, 112.0, 126.1, 134.1, 136.1, 141.7, 147.0, 161.8; IR (KBr, cm^{-1}) ν_{max} 3201 (NH), 2934, 2852 (alkane CH stretch), 1664 (amide C=O stretch), 1604, 1572, 1491, 1462, 1449, 1424; MALDI-MS calcd for $C_{26}H_{28}N_6O_2$ (M) 456.2; Found 456.2. HRMS (ESI): calcd. For $C_{26}H_{29}N_6O_2$ $[M + H]^+$ 457.2352; found 457.2338.

4.7. 8. Pip-B-DPP. A mixture of Pip-DPP (91.3 mg, 0.2 mmol) and triphenylborane (242 mg, 5.0 mmol) in toluene (8.0 mL) was stirred for 24 h at reflux under nitrogen atmosphere. After

cooling to room temperature, the mixture was evaporated to dryness in vacuo. The mixture was filtered and washed with Methanol and ethyl acetate and dried under vacuum. The product was isolated by column chromatography on silica gel using $CHCl_3$/methanol (10/1) as an eluent. Yield: 94.2 mg, 60%. ^{1}H NMR (400 MHz, $CDCl_3$) δ = 1.66 (s, 12H), 3.31 (s, 8H), 7.23-7.30 (m, 14H), 7.42 (d, 8H, *J* = 6.4 Hz), 7.88 (d, 2H, *J* = 2.4 Hz), 8.22 (d, 2H, *J* = 9.2 Hz); IR (KBr, cm^{-1}) ν_{max} 3051, 3005 (aromatic C-H stretch), 2936, 2846 (alkane CH stretch), 1635 (C=O amide stretch), 1604, 1558, 1500, 1431; MALDI-MS calcd for $C_{50}H_{47}B_2N_6O_2$ $[M+H]^+$ 785.4; Found 785.5. HRMS (ESI): calcd. For $C_{50}H_{47}B_2N_6O_2$ $[M + H]^+$ 785.3947; found 785.3972.

Table 4
Summarized crystallographic data

	H-B-DPP	H-Pt-DPP
Empirical Formura	$C_{42}H_{30}B_2Cl_6N_4O_2$	$C_{38}H_{46}N_4O_6Pt_2$ ·2$CHCl_3$,C_6H_{14}
Formula Weight	857.06	1369.92
Crystal Color	purple	mazarine
Crystal System	triclinic	monoclinic
a [Å]	8.6342(9)	15.815(3)
b [Å]	9.1785(9)	15.469(2)
c [Å]	13.483(2)	10.9272(17)
α [°]	103.0880(10)	
β [°]	93.3030(10)	102.665(2)
γ [°]	102.9130(10)	
V [Å^3]	1007.7(2)	2608.2(7)
Space Group	*P*-1 (#2)	$P2_1/c$ (#14)
Z value	1	2
$D_{calcd.}$ [g cm^{-3}]	1.412	1.744
F(000)	438.00	1344.00
μ (Mo-*Kα*) [cm^{-1}]	4.684	56.914
No. of reflections measured	total: 11504 unique: 4350 (R_{int} = 0.1613)	total: 26186 unique: 5618 (R_{int} = 0.021)
Reflection/parameter ratio	17.19	19.37
R_1 [$I > 2.00\sigma(I)$]	0.1125	0.0389
R (All reflections)	0.1226	0.0517
wR_2 (all reflections)	0.3352	0.0932
Goodness-of-fit Indicator	1.488	1.217

Acknowledgments

The authors thank the Chemical Analysis Center of the University of Tsukuba for the measurement of NMR, ESI-MS, MALDI-TOF-MS, X-ray, and elemental data.

Supplementary data

Supplementary data associated with this article can be found in the online version.

References

1. (a) Fischer, G. M.; Ehlers, A. P.; Zumbusch, A.; Daltrozzo, E. *Angew. Chem. Int. Ed.* **2007**, *46*, 3750-3753; (b) Fischer, G. M.; Isomäki-Krondahl, M.; Göttker-Schnetmann, I.; Daltrozzo, E.; Zumbusch, A. *Chem. Eur. J.* **2009**, *15*, 4857-4864; (c) Fischer, G. M.; Klein, M. K.; Daltrozzo, E.; Zumbusch, A. *Eur. J. Org. Chem.* **2011**, 3421-3429; (d) Berezin, M. Y.; Akers, W. J.; Guo, K.; Fischer, G. M.; Daltrozzo, E.; Zumbusch, A.; Achilefu, S. *Biophys. J.* **2009**, *97*, L22-L24; (e) Fischer, G. M.; Jüngst, C.; Isomäki-Krondahl, M.: Gauss, D.; Möller, H. M.; Daltrozzo, E.; Zumbusch, A. *Chem. Commun.* **2010**, *46*, 5289-5291; (f) Shimizu, S.; Iino, T.; Araki, Y.; Kobayashi, N. *Chem. Commun*. **2013**, *49*, 1621-1623.
2. Yamagata, T.; Kuwabara, J.; Kanbara, T. *Tetrahedron Lett*. **2010**, *51*, 1596-1599.
3. (a) Schutting, S.; Borisov, S. M.; Klimant, I. *Anal. Chem.* **2013**, *85*, 3271-3279; (b) Zhang, G.; Li, H.; Bi, S.; Song, L.; Lu, Y.; Zhang, L.; Yu, J.; Wang, L. *Analyst* **2013**, *138*, 6163-6170; (c) Zhang, G.; Bi, S.; Song, L.; Wang, F.; Yu, J.; Wang, L. *Dyes Pigm.* **2013**, *99*, 779-786; (d) Jeong, Y.-H.; Lee, C.-H.; Jang, W.-D. *Chem. Asian J.* **2012**, *7*, 1562-1566; e) C. Yang, M. Zheng, Y. Li, B. Zhang, J. Li, L. Bu, W. Liu, M. Sun, H. Zhang, Y. Tao, S. Xue, W. Yang, *J. Mater. Chem. A* **2013**, *1*, 5172-5178; f) Y. Qu, S. Qu, L. Yang, J. Hua, D. Qu, *Sensor and Actuators B* **2012**, *173*, 225-233.
4. (a) Tieke, B.; Rabindranath, A. R.; Zhang, K.; Zhu, Y. *Beilstein J. Org. Chem*. **2010**, *6*, 830-845. b) Suna, Y.; Nishida, J.; Fujisaki, Y.; Yamashita, Y. *Chem. Lett*. **2011**, *40*, 822-824; (c) Qiao, Y.; Guo, Y.; Yu, C.; Zhang, F.; Xu, W.; Liu, Y.; Zhu, D. *J. Am. Chem. Soc*. **2012**, *134*, 4084-4087; (d) Suna, Y.; Nishida, J.; Fujisaki, Y.; Yamashita, Y. *Org. Lett.* **2012**, *14*, 3356-3359; (e) Liu, S.-Y.; Li, H.-Y.; Shi, M.-M.; Jiang, H.; Hu, X.-L.; Li, W.-Q.; Fu, L.; Chen, H.-Z. *Macromolecules* **2012**, *45*, 9004-9009; (f) Liu, H.; Jia, H.; Wang, L.; Wu, Y.; Zhan, C.; Fu, H.; Yaoa, J. *Phys. Chem. Chem. Phys*. **2012**, *14*, 14262-14269.
5. (a) Jung, J. W.; Liu, F.; Russell, T. P.; Jo, W. H. *Chem. Commun*. **2013**, *49*, 8495-8497; (b) Deng, Y.; Chem, Y.; Liu, J.; Liu, L.; Tian, H.; Xie, Z. *ACS Appl. Mater. Interfaces* **2013**, *5*, 5741-5747; (c) Naik, M. A.; Patil, S. *J. Polym. Sci. A. Polym. Chem.* **2013**, *51*, 4241-4260; (d) Nielsen, C. B.; Ashraf, R. S.; Schroeder, B. C.; D'Angelo, P.; Watkins, S. E.; Song, K.; Anthopoulosb, T. D.; McCullocha, I.; *Chem. Commun.* **2012**, *48*, 5832-5834; (e) Qu, S.; Tian, H. *Chem. Commun*. **2012**, *48*, 3039-3051.
6. (a) Kuwabara, J.; Yamagata, T.; Kanbara, T. *Tetrahedron* **2010**, *66*, 3736-3741; (b) Yamagata, T.; Kuwabara, J.; Kanbara, T. *Eur. J. Org. Chem*. **2012**, 5282-5290.
7. (a) Luňák Jr., S.; Eliáš, Z.; Mikyek, T.; Vyňuchal, J.; Ludvík, J. *Electrochim Acta* **2013**, *106*, 351-359; (b) Bürckstümmer, H.; Weissenstein, A.; Bialas, D.; Würthner, F. *J. Org. Chem.* **2011**, *76*, 2426-2432; c) Liu, S.-Y.; Shi, M.-M.; Huang, J.-C.; Jin, Z.-N.; Hu, X.-L. *J. Mater. Chem. A*, **2013**, *1*, 2795-2805.
8. (a) Lorenz, I.-P.; Limmert, M.; Mayer, P.; Piotrowski, H.; Langhals, H.; Poppe, M.; Polborn, K. *Chem. Eur. J*. **2002**, *8*, 4047-4055. (b) Langhals, H.; Limmert, M.; Lorenz, I.-P.; Mayer, P.; Piotrowski, H.; Polborn, K. *Eur. J. Inorg. Chem.* **2000**, 2345-2349.
9. Grzybowski, M.; Glodkowska-Mrowka, E.; Stoklosa, T.; Gryko, D. T. *Org. Lett*. **2012**, *14*, 2670-2673.
10. Fukuzawa, A.; Yamaguchi, S. *Chem. Asian. J.* **2009**, *4*, 1386-1400.
11. (a) Wakamiya, A.; Taniguchi, T.; Yamaguchi, S. *Angew. Chem. Int. Ed.* **2006**, *45*, 3170-3173; (b) Fukazawa, A.; Yamaguchi, S. *Chem. Asian J.* **2009**, *4*, 1386-1400; (c) Li, D.; Yuan, Y.; Bi, H.; Yao, D.; Zhao, X.; Tian, W.; Wang, Y.; Zhang, H. *Inorg. Chem.* **2011**, *50*, 4825-4831; (d) Araneda, J. F.; Piers, W. E.; Heyne, B.; Parvez, M.; McDonald, R. *Angew. Chem. Int. Ed*. **2011**, *50*, 1-5; (e) Curiel, D.; Más-Montoya, M.; Usea, L.; Espinosa, A.; Orenes, R. A.; Molina, P. *Org. Lett.* **2012**, *14*, 3360-3363.
12. Shaabani, A.; Dabiri, M.; Bazgir, A.; Gharanjig, K. *Dyes Pigm.* **2006**, *71*, 68-72.
13. Imoda, T.; Hirota, T.; Takahashi, H.; Mizuguchi, J. *Acta Cryst*. **2005**, *E61*, o616-o618.
14. (a) Luňák, Jr. S.; Vyňuchal, J.; Vala, M.; Havel, L.; Hrdina, R. *Dyes Pigm.* **2009**, *82*, 102-108; (b) Vala, M.; Vyňuchal, J.; Toman, P; Weiter, M.; Luňák, Jr. S. *Dyes Pigm.* **2010**, *84*, 176-182; (c) Vala, M.; Weiter, M.; Vyňuchal, J.; Toman, P.; Luňák, Jr. S. *J. Fluoresc.* **2008**, *18*, 1181-1186.
15. Gaussian 09, Revision B.01, Frisch, M. J.; Trucks, G. W.; Schlegel, H. B.; Scuseria, G. E.; Robb, M. A.; Cheeseman, J. R.; Scalmani, G.; Barone, V.; Mennucci, B.; Petersson, G. A.; Nakatsuji, H.; Caricato, M.; Li, X.; Hratchian, H. P.; Izmaylov, A. F.; Bloino, J.; Zheng, G.; Sonnenberg, J. L.; Hada, M.; Ehara, M.; Toyota, K.; Fukuda, R.; Hasegawa, J.; Ishida, M.; Nakajima, T.; Honda, Y.; Kitao, O.; Nakai, H.; Vreven, T.; Montgomery, J. A., Jr.; Peralta, J. E.; Ogliaro, F.; Bearpark, M.; Heyd, J. J.; Brothers, E.; Kudin, K. N.; Staroverov, V. N.; Kobayashi, R.; Normand, J.; Raghavachari, K.; Rendell, A.; Burant, J. C.; Iyengar, S. S.; Tomasi, J.; Cossi, M.; Rega, N.; Millam, N. J.; Klene, M.; Knox, J. E.; Cross, J. B.; Bakken, V.; Adamo, C.; Jaramillo, J.; Gomperts, R.; Stratmann, R. E.; Yazyev, O.; Austin, A. J.; Cammi, R.; Pomelli, C.; Ochterski, J. W.; Martin, R. L.; Morokuma, K.; Zakrzewski, V. G.; Voth, G. A.; Salvador, P.; Dannenberg, J. J.; Dapprich, S.; Daniels, A. D.; Farkas, Ö.; Foresman, J. B.; Ortiz, J. V.; Cioslowski, J.; Fox, D. J. Gaussian, Inc., Wallingford CT, 2009.

16. (a) Oakley, S. R.; Nawn, G.; Waldie, K. M.; MacInnis, T. D.; Patrick, B. O.; Hicks, R. G. *Chem. Commun*. **2010**, *46*, 6753-6755; (b) Nawn, G.; Waldie, K. M.; Oakley, S. R.; Peters, B. D.; Mandel, D.; Patrick, B. O.; McDonald, R.; Hicks, R. G. *Inorg. Chem*. **2011**, *50*, 9826-9837; (c) Nawn, G.; Oakley, S. R.; Majewski, M. B.; McDonald, R.; Patrick, B. O.; Hicks, R. G. *Chem. Sci*. **2013**, *4*, 612–621; (d) Nawn, G.; McDonald, R.; Hicks, R. G. *Inorg. Chem*. **2013**, *52*, 10912-10919.
17. Bürckstümmer, H.; Weissenstein, A.; Bialas, D.; Würthner, F. *J. Org. Chem.* **2011**, *76*, 2426-2432.
18. Han, X.; Wu, L.; Zhang, L.; Tung, C. *Chinese Science Bulletin* **2006**, *51*, 1005-1009.